Seventh South African Conference on Computational and Applied Mechanics
SACAM10
Pretoria, 10–13 January 2010

Velocity Flow Field and Water Level Measurements in Shoaling and Breaking Water Waves

R. Mukaro[*,1], K. Govender[*,2] , I Gledhill[†,] N.L. Kokwe[*,3]

[*]School of Physics
University of KwaZulu-Natal, Private Bag X54001, Durban, South Africa,
[1]mukaror@ukzn.ac.za, [2]govenderks@ukzn.ac.za, [3]njabulo123@gmail.com

[†]CSIR, Meiring Naude Dr, Pretoria, South Africa
igledhil@csir.co.za

Abstract

In this paper we report on the laboratory investigations of breaking water waves. Measurements of the water levels and instantaneous fluid velocities were conducted in water waves breaking on a sloping beach within a glass flume. Instantaneous water levels were measured using capacitive waves gauges, while the instantaneous velocity flow fields were measured using video techniques together with digital correlation techniques. The instantaneous velocity flow fields were further analyzed to yield turbulence intensities, turbulent kinetic energies and vorticity.

Keywords: breaking waves, digital correlation image velocimetry (DCIV), velocity flow fields, turbulence intensities, vorticity.

1. Introduction

The coastal regions (surf zone) of the oceans are characterized by breaking waves, in which the wave energy is converted to turbulence and currents. These turbulence and currents are responsible for the erosion and sometimes destruction of coastlines and coastal structures. With the view to protecting harbors and certain coastal structures, break-water structures such as the dolos are frequently used. The equations describing the processes occurring in breaking waves are highly nonlinear and are often intractable. The analysis of the interaction of waves with break-water structures is further complicated by the complex geometries that are involved. Therefore, in order to predict the effects of breaking waves, a number of averaged quantities, such as mass and momentum fluxes, radiation stress and mean water level to name a few, are defined and a set of equations based on these averaged quantities are frequently used.

Turbulence is recognized as irregularly fluctuating and unpredictable motion which is composed of a number of small eddies that travel in the current. Turbulence is ubiquitous but its measurement has not been easy. It is natural that, in spite of the difficulty involved, turbulence has attracted the attention of engineers and physicists because of its practical importance in applications such as weather forecasting, aeronautical engineering, etc.

Understanding mixing is especially important for ocean models designed to predict global circulation, climate change, pollutant dispersal and primary productivity. Without turbulence and the mixing it causes, we would not have the same ocean that we do now, nor indeed the same climate. Turbulent mixing brings nutrients into the surface layer from below so that plankton can grow. Turbulence near the surface, driven by surface winds and cooling, transmits heat in and out of the ocean to create the reservoir of heat that governs climate. Turbulence in the bottom layer affects the deposition, resuspension and movement of sediments and creates micro-environments for the small creatures that form the basis for life in the oceans. For the above

reasons and more, an improved knowledge of fluid dynamics of breaking is vital to better understand air-sea interactions from micro to global scales (Melville et al, 2002, Banner and Perregrine,1993). A treatment of turbulence naturally leads to a discussion about statistics of the flow (usually velocity) and their relation to the flow Reynolds number *Re*. Various investigators have used different contact-free measuring techniques like laser Doppler anemometry (LDA) and particle image velocimetry (PIV) to get a real insight into the mechanics of breaking waves (Liiv & Lagemaa,2008). Chang and Liu, xx measured the kinematics of the breaking waves and found that the velocity of the water particles in the wave crest exceeded the wave phase velocity 1.7 times.

With increasing knowledge of the breaking process, mathematicians and computational physicists alike have proposed several mathematical models to describe turbulence. A common problem is that for accurate representation of the physical phenomenon, the model equations have to contain non-linear terms, and therefore it is necessary to use empirical relations that can only be obtained through experiments. Fedder & Trowbridge(2005) measured the wave generated turbulence in the surf zone and developed a model that is able to reproduce the production and dissipation of turbulence during wave breaking.

The objectives of the present series of experiments are to provide greater insights, especially in the upper parts of breaking waves, and to examine the interaction of waves with submerged obstacles. These experimental results are being used to calibrate wave models developed using computational fluid dynamics integrated with object models developed using a physics engine Grobler et al. [1]. In this paper we report on experiments using regular two-dimensional waves breaking on a plane slope beach in a glass walled flume. The velocity flow fields at various positions along the flume were measured using digital correlation image velocimetry (DCIV). By tracking the motion of neutrally buoyant particles, as well as bubble structures within the crest of the wave, we were able to measure velocities well into the crest of the wave. The validation of this measurement method and further results can be found in Govender et al. [2, 3] . The experimental setup for this purpose is as follows: a longitudinal section of the flume was illuminated with a strobed light sheet, and the aeration/bubble structure and illuminated particles were imaged using a progressive scan CCD camera connected to a frame grabber residing in a PC. Video images are captured and downloaded to the frame grabber using standard TV rates. While a particular frame is being acquired (or exposed), the previous frame is downloaded to the frame grabber. By means of a unique strobing of the light sheet, two video images of the aerated and seeded flow, which are separated in time by a few milliseconds (less than one frame time), are captured. The instantaneous velocity field is obtained by subdividing each image into smaller sub-images and then cross correlating the sub image in one video frame with the corresponding sub image in the second video frame. The mean and fluctuating velocity fields are obtained by means of phase ensemble averaging. The estimates of these instantaneous and fluctuating velocities together with preliminary analysis of the averaged vorticity will be presented.

The organization of the paper is as follows: Section 2 provides the necessary equations and definitions used in the data analysis. Section 3 gives details of the experimental setup and computational procedures, and the results are provided in Section 4.

2. Theory

In this section the basic equations and definitions that are used in the analysis of the experimental data is provided. In the study of turbulent flow involving periodic waves there are two types of averaging that is used. The first is phase ensemble averaging. This is an average of a quantity at a particular point (or phase) within the wave cycle. This is achieved by measuring the relevant quantity at a particular phase of the wave over a number of wave cycles. This type of averaging will be denoted by angle brackets. The second type of

averaging is time averaging. This is the average over a full wave cycle of the phase-ensemble averaged quantity and will be denoted by means of an over bar.

2.1 Turbulence fluctuations and ensemble average

The turbulent flow velocity can be described as a sum of the averaged velocity and the fluctuating component :

$$u_i(x,y,z,\theta,t) = \langle u_i(x,y,z,\theta,t)\rangle + u_i'(x,y,z,\theta,t) \quad (1)$$

where $u_i(x,y,z,\theta,t) = (u_x(x,y,z,\theta t), u_y(x,y,z,\theta,t), u_z(x,y,z,\theta,t))$ is the measured velocity, $\langle u_i(x,y,z,\theta,t)\rangle$ is the phase-ensemble averaged velocity and $u_i'(x,y,z,\theta,t)$ reflects the instantaneous turbulent fluctuations, (*x*,*y*,*z*) represents position within the flume relative to some chosen coordinate system and θ represents the phase within a wave cycle.

The phase-ensemble-averaged velocity is calculated using:

$$\langle u_i(x,y,z,\theta,t)\rangle = \frac{1}{N}\sum_{i-0}^{i=N-1} u_i(x,y,z,\theta,t) \quad (2)$$

where N is the number of samples captured at a particular phase.
The turbulent fluctuation is usually quantified by the turbulent intensity, which is the root mean square of fluctuation, and computed as follows:

$$\sqrt{\langle u_i'(x,y,z,\theta,t)^2\rangle} = \sqrt{\frac{1}{N}\sum_{i=0}^{i=N-1}\left(u_i(x,y,z,\theta,t) - u\langle_i(x,y,z,\theta,t)\rangle\right)^2} \quad (3)$$

In the remainder of the paper the primed turbulent velocity components will be used to represent the root mean square values of the turbulent fluctuations as given by equation (3).

2.2 Turbulent kinetic Energy

The phase-ensemble -average turbulent kinetic energy (TKE) per unit mass is defined as follows :

$$\langle k\rangle = \frac{1}{2}\left(u_x'^2 + u_y'^2 + u_z'^2\right) \quad (4)$$

Now in measurements were only two components (u_x and u_z) are measured, turbulence in the surf zone can be estimated as suggested by Svendsen(1987) and Liiv & Lagemaa(2002) as follows:

$$\langle k\rangle = \frac{1.33}{2}\left(u_x'^2 + u_z'^2\right) \quad (5)$$

2.3 Vorticity

Vorticity of a fluid is an important factor in fluid dynamics and mechanics and is a natural way to describe turbulence. Certain coherent features of turbulent flows are visible in the vorticity field, even though the velocity field may appear to be 'chaotic'. Vorticity is a measure of rotational spin in a fluid and is mathematically defined as the curl of the velocity field. In physical terms, the vorticity of a parcel of fluid is the curl of the velocity field:

$$\vec{\omega} = \vec{\nabla} \times \vec{u} = \vec{i}\left(\frac{\partial u_z}{\partial y} - \frac{\partial u_y}{\partial z}\right) + \vec{j}\left(\frac{\partial u_x}{\partial z} - \frac{\partial u_z}{\partial x}\right) + \vec{k}\left(\frac{\partial u_y}{\partial x} - \frac{\partial u_x}{\partial y}\right) \quad (6)$$

where the *x*, *y* and *z* indices denote the respective orthogonal directions and *i*, *j* and *k* are the unit basis vectors for the three-dimensional Euclidean space R^3, and *u* is the vector field (u_x, u_y, u_z), and are functions of the variables *x*, *y*, and *z* (which denote the respective orthogonal directions).

A vortex can be described as a fluid structure that possesses circular or swirling motion. Therefore, vorticity (the curl of the velocity field) represents the skeleton of the flow field and the principal quantity to define the flow structure (Kim *et al*, 1995 ; Wu *et al*, 2006).

If we consider a two-dimensional fluid flow in the x-z plane, the vorticity component, which points in the y -direction is given:

$$\omega_y = \frac{\partial u_x}{\partial z} - \frac{\partial u_z}{\partial x} \quad (7)$$

The vorticity field ω is computed with the derivatives of each velocity component (u_x and u_z). Several numerical schemes exist for performing this calculation. The central difference method is the mostly adopted method especially when dealing with PIV measurements affected by a non-negligible noise level and is used here to estimate vorticity as follows :

$$\omega = \left(\frac{u_x(i,\, j+1) - u_x(i,\, j-1)}{2\Delta z}\right) - \left(\frac{u_z(i+1,\, j) - u_z(i+1,\, j)}{2\Delta x}\right) \quad (8)$$

where Δx and Δz are the x and z-grid spacing, respectively and $u_{x,z}(i,j)=u_{x,z}(i\,\Delta x\,,\, j\Delta z)$ and *i* and *j* are integers.

3. Experimental Setup

The experiments were conducted in a glass-walled flume in the Coastal Engineering Laboratory at CSIR, Stellenbosch, South Africa to study the variation of the 2-D flow fields during the breaking process. For this purpose, regular waves were generated in the wave flume. Vertical and horizontal velocity components under strongly plunging breaking waves were measured using what Govender et al.,(2002) called digital correlation image velocimetry (DCIV).

Figure 1 shows a schematic of the flume. The flume is approximately 20 m long, 0.5 m wide and has a beach slope of 1:20. At one end of the flume is a computer-controlled wave maker. The waves were generated using a piston type wave paddle manufactured by HR Wallingford that is equipped with an active wave absorption control system . The wave maker has a maximum paddle stroke of 0.8 m and is designed for water depths of up to 0.75 m. Complementary documentation of wave maker specifications and wave generation mechanism may be found in [4].

At the other end of the flume a beach covered with quarry stones absorbed any wave energy remaining after breaking. Waves of frequency 0.7 Hz and having a wave height 0.16m in the flat section of the flume were used. This resulted in a plunging wave which broke approximately 4.5m

from the still water mark on the beach. Before the measurement procedures were initiated, the waves were allowed to run for 30 min to ensure steady state conditions were reached.

Surface displacements were measured using capacitive wave gauges which were sampled at rate of 20 kHz for 2 minutes giving a total of 2400 samples for each probe. These three probes are labeled P_1, P_2 and P_3 in Figure 1. These three probes were initially located at distance 2.50 m, 4.65 m and 7.25 m from the still water mark on beach, respectively and was moved in steps of 10cm across the flume to measure the instantaneous water levels. The breaking point of the wave was determined by visual observations and by examining a plot of wave height versus position along the flume.

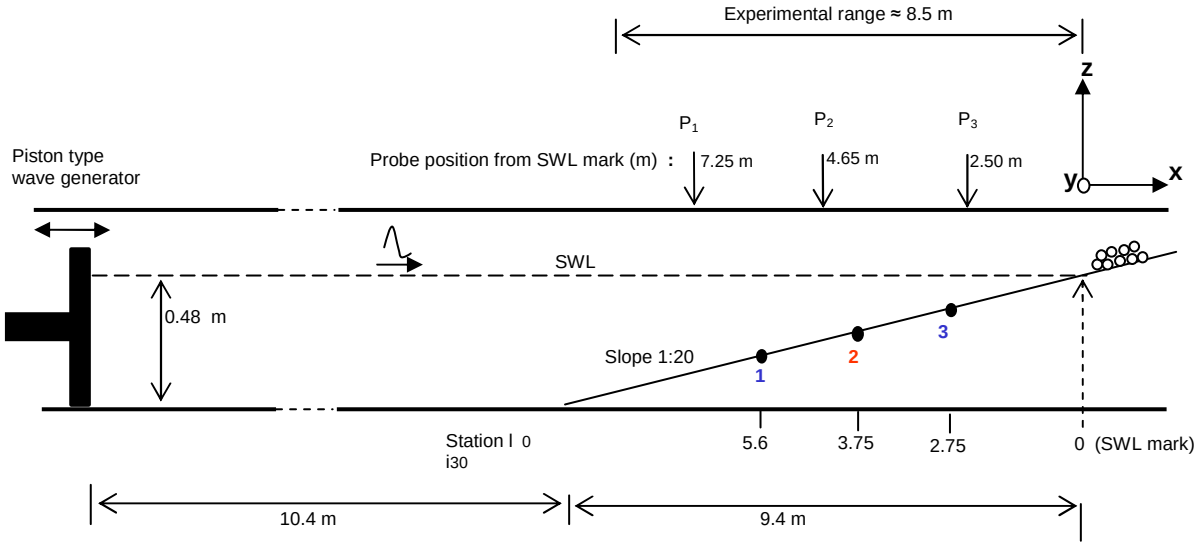

Fig. 1 Schematic of the wave flume showing measurement stations and their location from the SWL mark on the beach. Water levels were measured every 10 cm over the experimental section starting at the positions indicated by probe positions, P_1 , P_2 and P_3, covering a range of about 8.5 m from the SWL mark. Velocities were measured at stations marked, 1, 2, and 3, located 5.6, 3.75 and 2.75 m, respectively from the swl mark. The wave breaks in the vicinity of station 2.

The experimental setup for velocity measurements is shown in Figure 2. A longitudinal section of the flume was illuminated with a strobed light sheet. The water was also seeded with partially expanded polystyrene beads. Pairs of images, separated a few millisecond, of the beads and aeration due to breaking were obtained by strobing the light sheet at the end of one video frame time and again at the beginning of the next.. The time between flashing of the light sheet correspond to the time between the images in each pair. The instantaneous velocity field is then obtained using each pair of images.

A trigger pulse from the generator made it possible to capture images at a particular wave phase. In our experiment we captured images at twenty equally spaced wave phases. At each wave phase a number of image pairs were captured over number of wave cycles. This enabled ensemble averaging to be conducted.

Fluid velocity measurements were conducted at the three stations marked 1, 2, and 3 in Figure 1, which were located 5.60 m , 3.75 and 2.75 m respectively from the still water mark on the beach. In this paper we report on measurements for station 2.

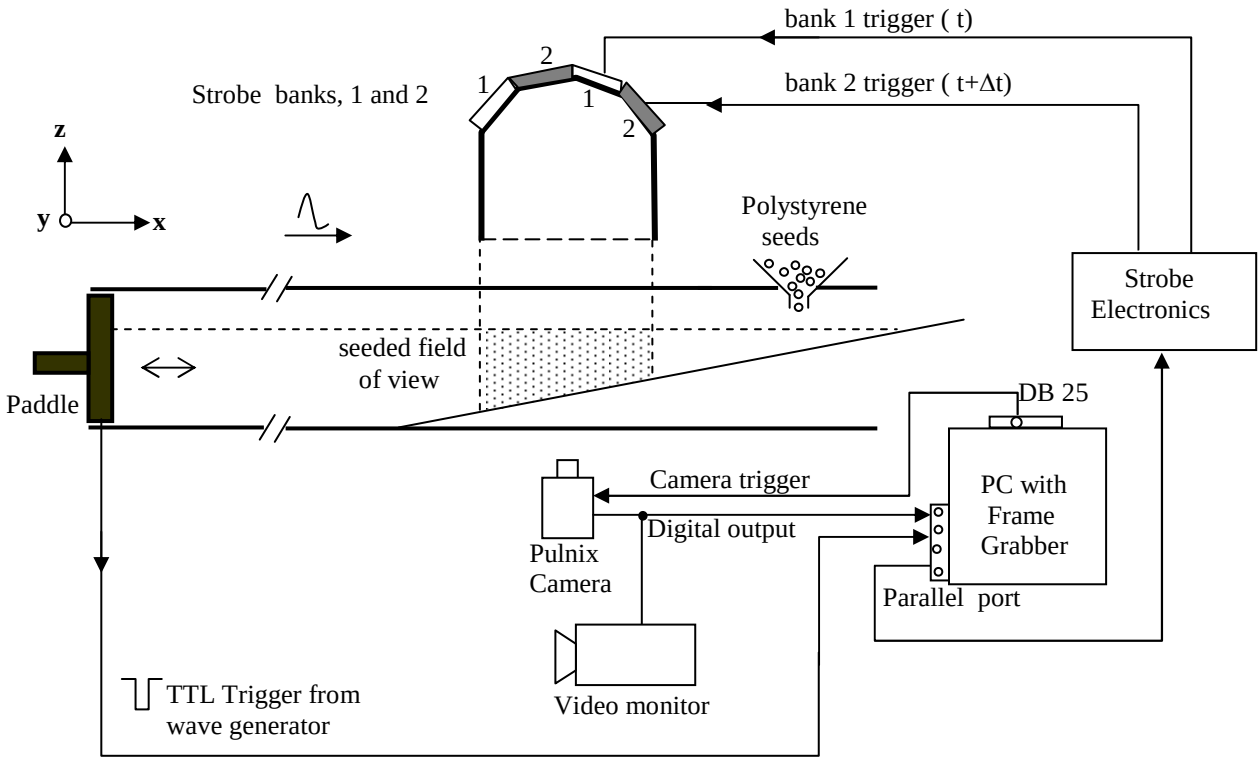

Fig .2 : Schematic of experimental setup for the DCIV measurement system used for studying turbulence in water waves breaking in a flume.

The instantaneous velocity field from each image pair was obtained as follows:
At a given point (*i*,*j*) in the first image an interrogation window of 32×32 pixels centered at *(i,j)* was placed. The sub-image contained within this interrogation window was then cross correlated with a corresponding sub image in the second image. The position of peak in the cross-correlation-result gives a measure of the displacement of the beads and or aeration structures between the subimages. Dividing the displacement by the time between images gives the velocity at the point (*i*,*j*) in the images.The interrogation window was moved in regular steps (8 pixels vertically and horizontally) across the entire image to obtain the velocity flow field over the entire image. The cross correlation was implemented using the Fast Fourier Transform (FFT) and the positions of the peak in the cross correlation was estimated with sub pixel resolution. Figure 3 illustrates the above procedure.

4. Results

4.1 Water level measurements

Figure 4 shows a sample of the instantaneous water levels at three positions along the flume, corresponding to near the generator, near the break point and in the breaking region. It is evident from the figure that has the waves move from deep to shallow water (due to the sloping bottom) the wave profile changes from being sinusoidal to being more peaked at the crest while the troughs become drawn out.

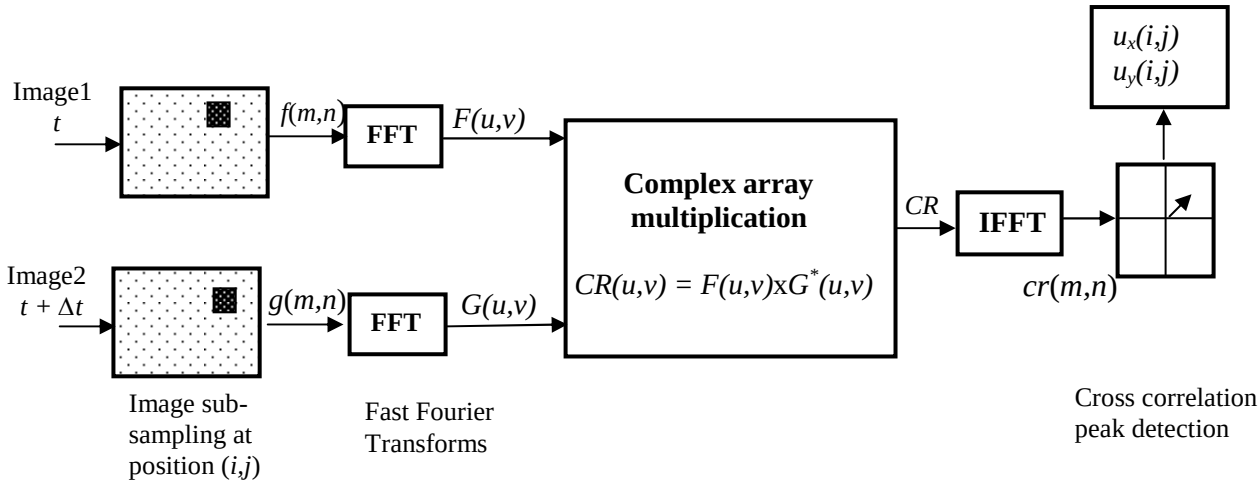

Fig. 3. Numerical processing flow-chart of Fourier cross-correlation procedure for DCIV measurements. (Willert & Gharib, 1991; Weng *et al*, 2001 ;)

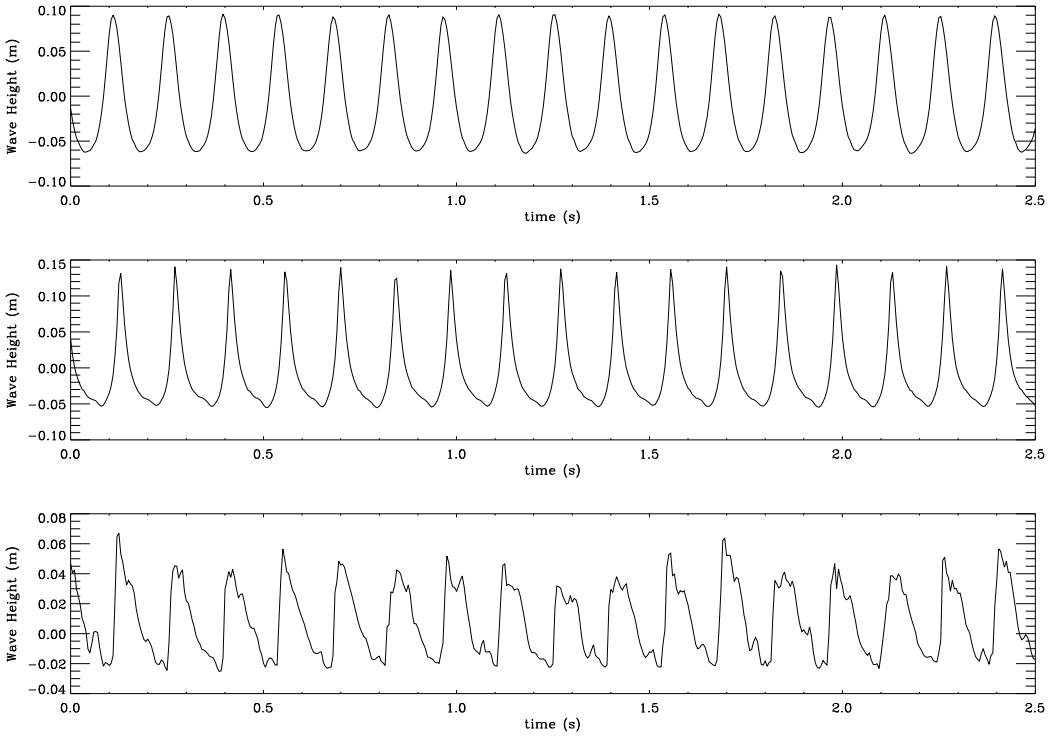

Figure 4. Time series of water levels near (top)-wave generator (middle)-breaking point and (bottom) – surf zone.

The variation of the wave height (mean vertical distance from the bottom of the troughs to the top of the crests) is shown in Figure 5. The wave height increases has the waves move into shallow water, reaching maximum at which breaking occurs. The wave height decreases thereafter. The reason for the increase during pre-breaking is due to the fact that the wave speed $c = \sqrt{gh}$, (where h is the local water depth and g is gravitational acceleration,) decreases as the waves move up the slope. However, since the energy flux is constant, the wave height has to increase. The decrease in wave height after breaking is due to loss of wave energy due to breaking.

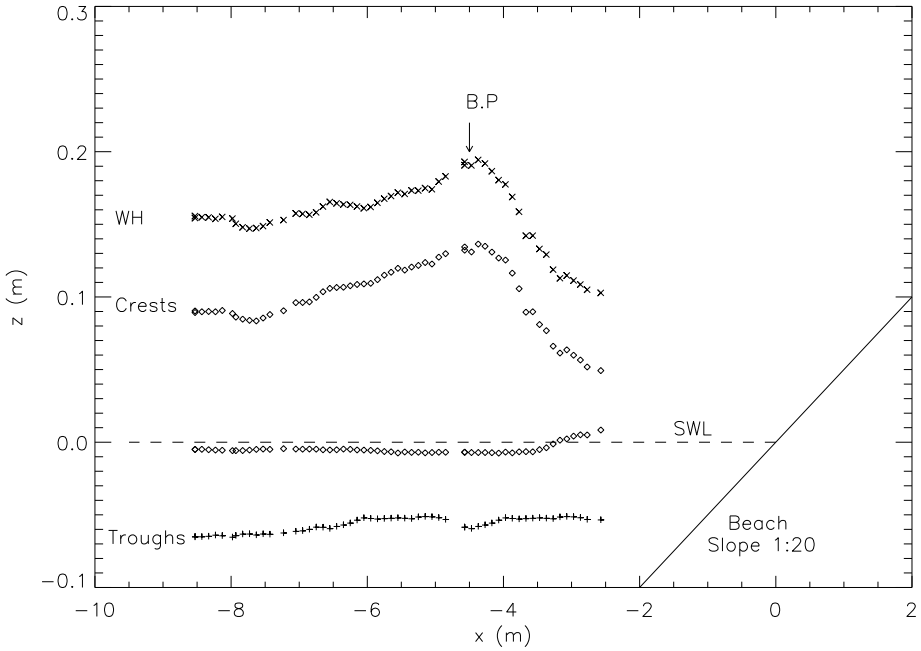

Figure 5 Waveheight measurements as a function of distance from the still water line (SWL) mark on the beach, for a 0.7 Hz plunging. Crests (◊), Troughs (+), Wave Height (x) and Mean Water Level (Δ) . The breaking point for the wave is at 4.5 m from the SWL mark.

Figure 6 shows a closer view of the variation of MWL across the flume. Clearly there is a lowering of the mean water level before breaking, called the set-down, and a rising of the mean water level after breaking, called the setup. In the real ocean the setup can translate to a few meters. A higher mean water level in the surf zone coupled with high levels of turbulence and currents will result in greater amount of erosion and sediment transport.

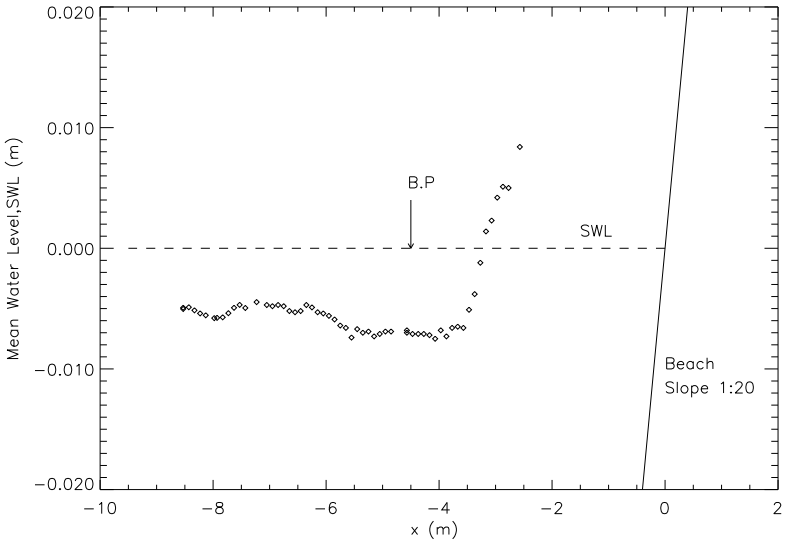

Figure 6. Mean Water Level (MWL) along the flume.

6.2 Velocity measurements

Our imaging setup can view only a small section of the wave at any time. In order to conduct measurement over the entire wave we imaged the wave at twenty equally spaced phase positions as follows: we begin with phase 0 and image a 38 cm section of the wave over a number of cycles, then we move to phase 1 and repeat the above measurement. This is repeated until all phases are covered. Recall that each image capture represents two imaged space a few milliseconds apart. All images were then analyzed to obtain the instantaneous velocity flow fields. The instantaneous velocity fields were further analyzed to extract turbulence intensities, turbulent kinetic energies (TKE) and vorticity.

Figure 7 shows images of the wave corresponding to 4 consecutive phases, but captured from different wave cycles.These images correspond to phases 10(extreme right), 11, 12 and 13(extreme left)

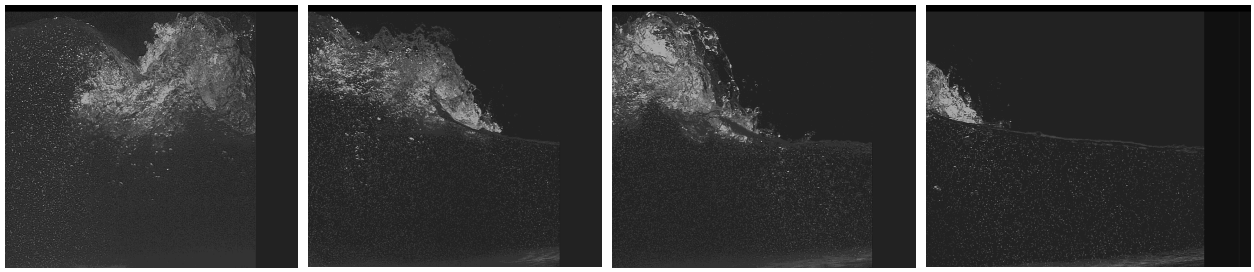

Figure 7: Image of waves corresponding to phase (from left to right) 13, 12, 11 and 10 at station 2. Note that the left edge of each image corresponds to 3.75m from the still water mark on the beach.

The instantaneous velocity field corresponding to phase 13 is shown in Figure 8. Clearly we are able to measure velocities over the entire image including the aerated portion of the waves, which is not possible using techniques such as LDA. The wave phase speed, using a mean depth corresponding to the middle of the images associated with station 2, is 1.32m/s. The instantaneous velocities in the upper part of the wave are approximately a factor of two greater than the phase speed. Phases 10 to 13 are the phases containing the most dynamic part of the wave. We will therefore show results pertaining to these phase positions. The

phase ensemble-averaged flow fields for phase 13 and 12 are shown in Figure 8(a) and (b), respectively. Figure 9 shows the horizontal and vertical turbulence intensities for phase 12. Figure 10 shows the vertical structure of the horizontal and vertical turbulence intensities. From these figures it is clear that the highest levels of turbulence occur in the crests of the wave. The turbulence intensities are approximately of same order of magnitude as the phase velocity.

Figure 8. Instantaneous velocity flow field corresponding to image associated with phase 13 in Figure 7.

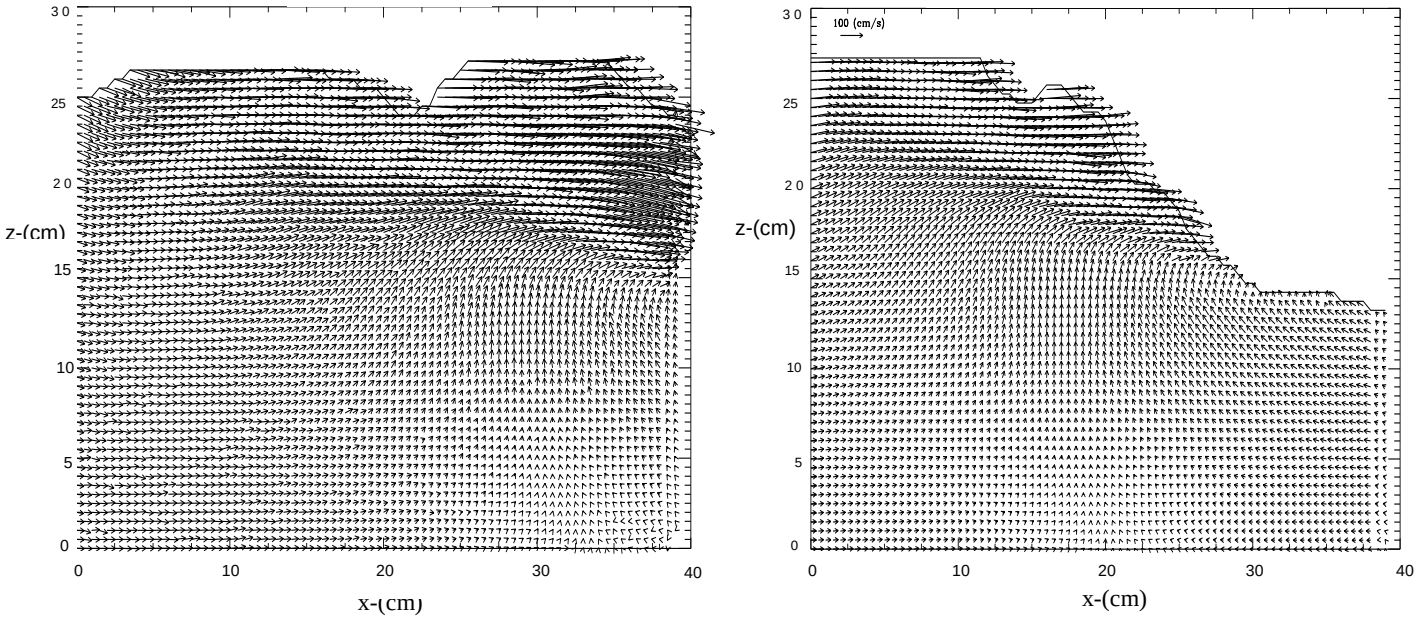

(a) (b)

Figure 9. Phase-ensemble average horizontal velocity at station 2 for (a) Phase 13 (b) Phase 12 . The continuous lines in the graphs shows the wave profiles.

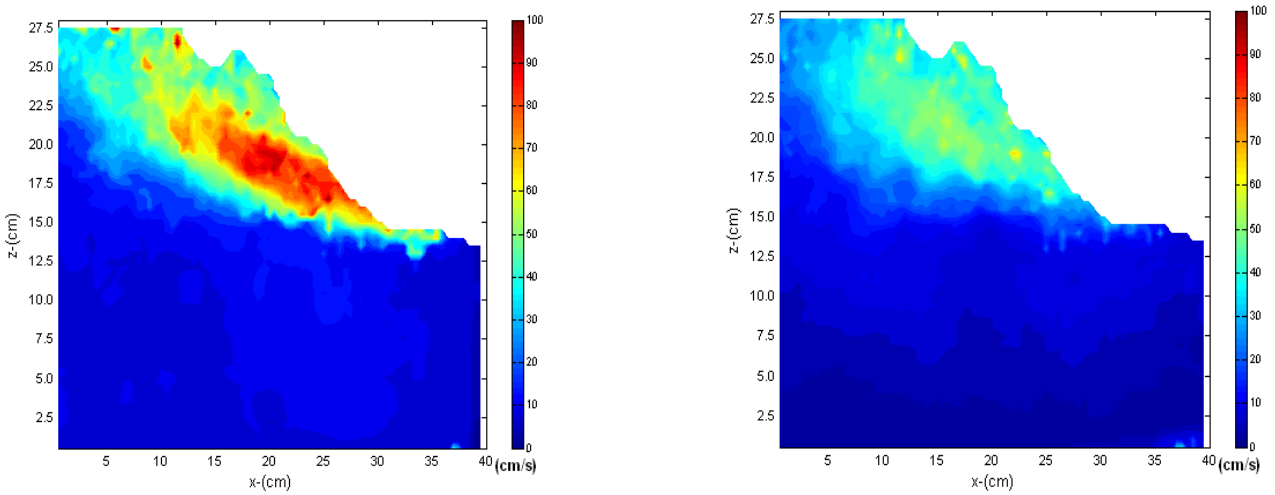

(a) (b)

Figure 10. Colour plots of phase-ensemble average (a) horizontal turbulence intensity u' (b) vertical turbulence intensity w' for phase 12. The colour code shows the magnitude of the mean turbulence intensity with a peak value of about 80 cm/s inside the crest.

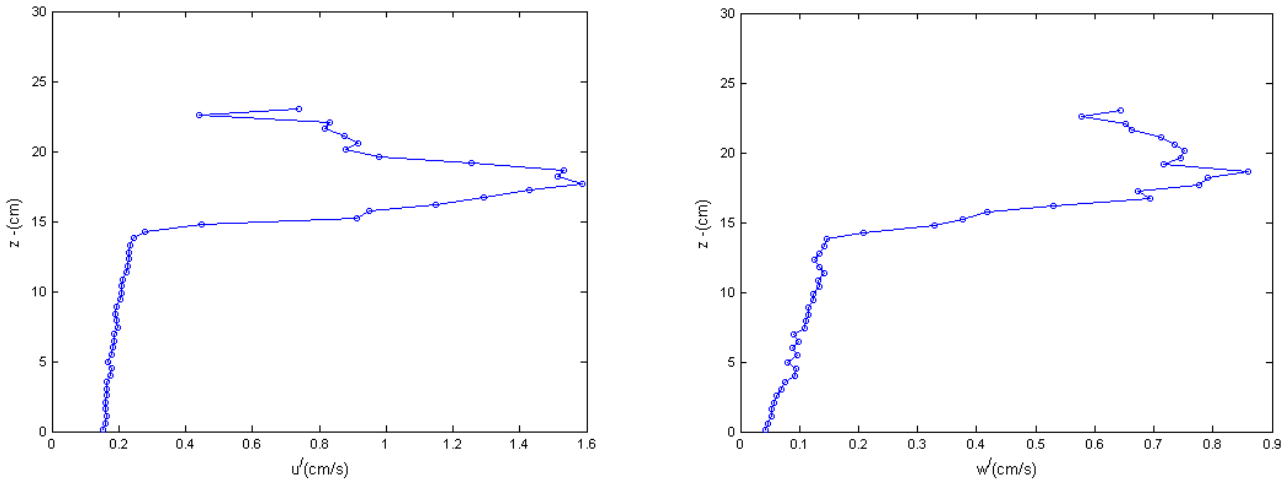

(a) (b)

Fig 11. Vertical structure of phase ensemble-averaged turbulent intensity , at x = 20 cm for (a) horizontal and (b) vertical The position z = 15 cm corresponds to the still water line (SWL).

6.4 Turbulent Kinetic Energy(TKE)

The computed TKE for phase 10 to 13 are shown in Figure 12. Once again high TKE values are observed near the front face of the wave. This region of high TKE values corresponds to what is called the wave roller. The wave roller is a body of fluid that rides on the front face of the wave.

Figure 13 shows the vertical structure of TKE at selected positions within each image. Peak TKE values of 7000 cm^2/s^2 are observed in the crests, while a value of around 100 cm^2/s^2 are observed near the bottom of the wave.

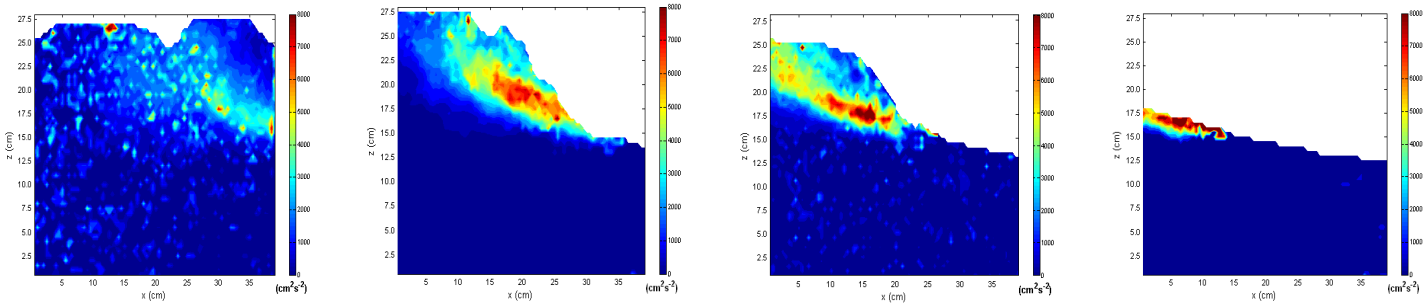

Fig 12. Turbulent Kinetic Energy for phases (from left to right)13, 12, 11 and 10.

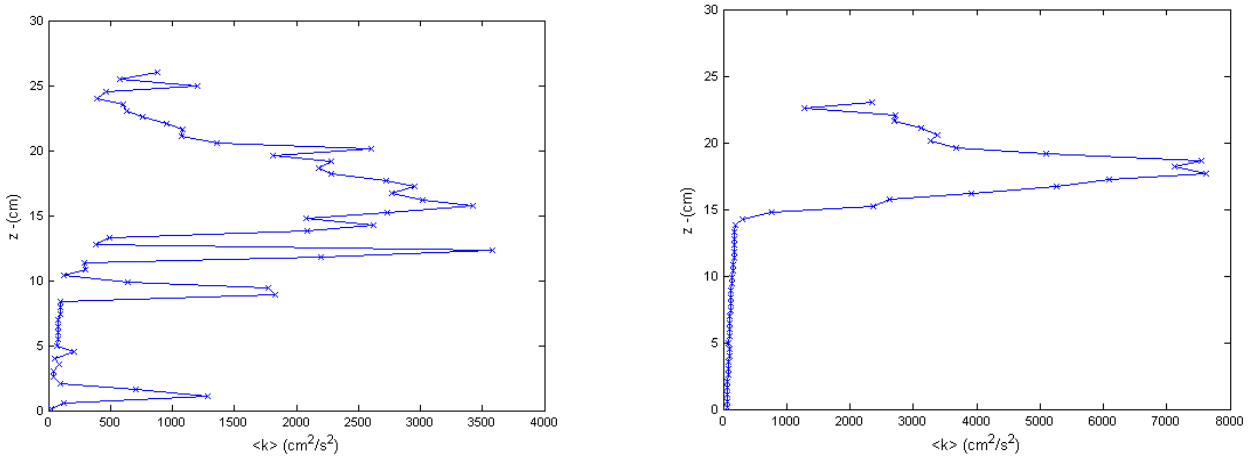

(a) (b)

Fig. 13. Vertical structure of phase ensemble-averaged turbulent kinetic energy, at (a) x = 35 cm for phase 13 (b) x = 20 cm for phase 12.

6.5 Vorticity

Figure 14 below shows the a colour plot of variation of vorticity for phases 10 to 13, while Figure 14 (a) and (b) show the vertical variation of vorticity at selected positions within the images of phase 13 and 12, respectively. Positive vorticity indicates motion in clockwise rotation and the direction is into the plane of the figure while negative vorticity indicates anticlockwise rotation with direction out of the plane of the figure. Near the front face of the wave vorticity is in the order of 80 s^{-1}, while in the rest of the wave it is negligible.

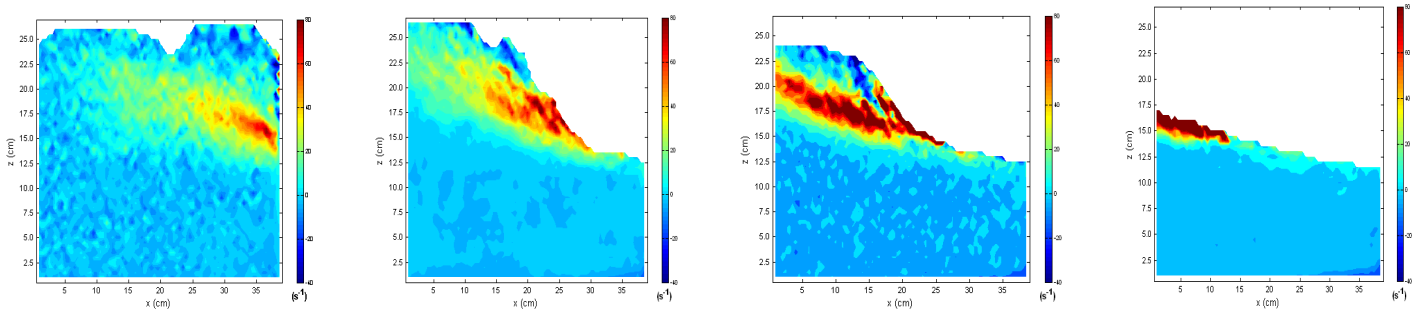

Fig 14. Vorticity of the phase ensemble averaged velocity flowfields corresponding to phases 13 to 10.

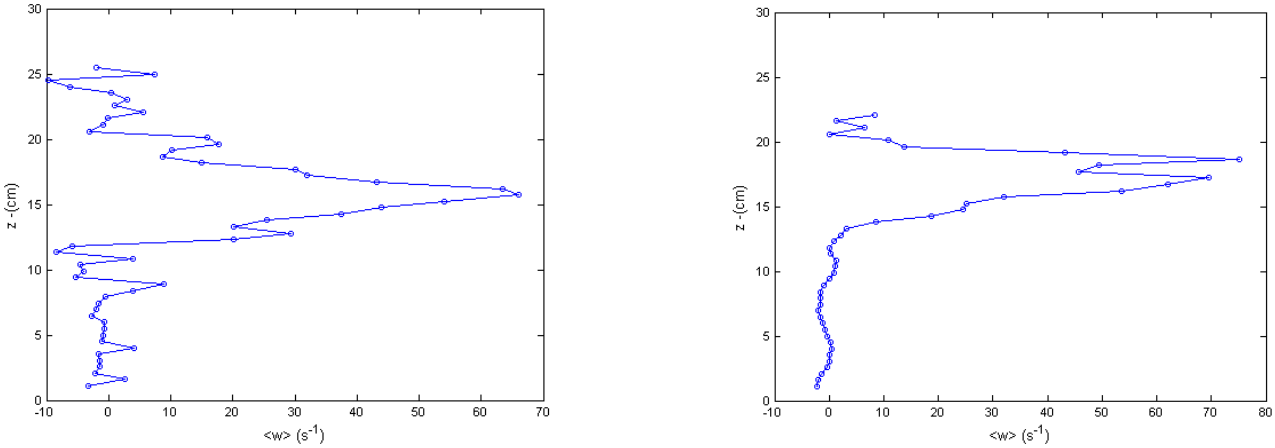

(a) (b)

Fig 15. Vertical structure of vorticity at (a) x = 35 cm for phase 13 and (b) x = 20 cm for phase 12

7. CONCLUSIONS

The results of an experimental study of water waves breaking in a laboratory surf zone have been presented. Fluid velocities were measured by tracking the motion of almost neutrally buoyant particles as well as aeration structures formed by breaking waves. Velocity measurement for one position along the surf zone was provided. The instantaneous velocities were further analyzed to yield turbulence intensities, turbulent kinetic energies. Peak turbulence intensities and turbulent kinetic energies were found to occur in the crest of the breaking waves

Coherent features were examined via vorticity computations of the phase-ensemble averaged velocity flow fields. High rotation rates were found to occur near the front face of water break waves, while in the rest of the wave vorticity was found to be minimal.

The data presented in this paper represents a unique set of measurements that spans the entire water column. These measurements will be valuable for validation of mathematical and computational fluid models of surf zone turbulence. Further results from the present series of experiments will be published in the near future.

8. References

[1] J.-H Grobler, R. De Villiers and A.K. Cooper, Modeling of fluid-solid interaction using two stand-alone codes. Submitted to the Seventh South African Conference on Computational and Applied Mechanics (SACAM10), Pretoria, 2010.

[2] K. Govender, M.J. Alport, G. Mocke, Video imaged surf zone wave and roller structures and flow fields. J. Geophy Res., 107(C7), 3072, doi:10.1029/2000JC000755, 2002.

[3] K. Govender, H. Michallet, M.J. Alport, U. Pillay, G.P. Mocke and M. Mory, Video DCIV measurements of mass and momentum fluxes and kinetic energies in laboratory waves breaking over a bar, Coastal Engineering, (56) 879-885, 2009.

[4] http://www.hrwallingford.co.uk/index.aspx?facets=equipment

[5] Hu H, Saga T, Kobayashi T, Okamoto K, and Taniguchi N (1998) ; Evaluation of cross-correlation method by using PIV standard images. Journal of Visualization, vol. 1, (1), 87-94.

[6] Weng W.G, W.C. Fan, G.X. Liao,J. Qin (2001) : Wavelet-based image denoising in (digital) particle image velocimetry, Signal Processing , 81, 1503-1512

[7] Willert C.E, M. Gharib (1991): Digital particle image velocimetry, Exp. Fluids, 10, 181-193.]

[8] Zeilstra C., J.G. Collignon, M.A. van der Hoef , N.G. Deen, J.A.M. Kuipers (2008) : Experimental and numerical study of wall-induced granular convection, Powder Technology 184,166–176.

[9] Westerweel J, Poelma C and Lindken R 2002 Two-point ensemble correlation method for μPIV applications *11th Int. Symp. on Applications of Laser techniques to Fluid Mechanics (Lisbon)*

[10] Wu JZ, Ma HY, Zhou, MD. Vorticity and Vortex DynamicsBerlin-Heidelberg, Germany: Springer-Verlag; 2006.

[11] Kim WY, Walker PG, Pedersen EM, et al. Left ventricular blood flow patterns in normal subjects: a quantitative analysis by three-dimensional magnetic resonance velocity mapping. J. Am. Coll. Cardiol., 1995;26:224-238.